Electron-conducting quantum-dot solids with ionic charge compensation

Aarnoud L. Roest, Arjan J. Houtepen, John J. Kelly and Daniël Vanmaekelbergh*

Chemistry and Physics of Condensed Matter, Debye Institute, University of Utrecht, P.O. Box 80000, 3508 TA Utrecht, The Netherlands

Received 11th March 2003, Accepted 20th May 2003
First published as an Advance Article on the web 13th October 2003

Electron-conducting quantum-dot solids can be prepared on the basis of assemblies of colloidal insulating nanocrystals if electrons can be injected in the delocalized conduction orbitals. We discuss the energetics of electron injection in such an artificial solid consisting of weakly coupled quantum dots. We show that quantum confinement and electron–electron repulsion determine the charging characteristics. The electron–electron repulsion energy can be screened by three-dimensional charge compensation from trapped holes or positive inert ions inserted in the assembly. We present experimental results on the electron storage and long-range transport in assemblies of ZnO nanocrystals in which the electron charge is compensated by positive ions. The electron–electron repulsion energy in assemblies permeated with an aqueous electrolyte solution is strongly screened. In contrast, the repulsion energy is about 100 meV in aprotic solvents; the repulsion energy strongly influences electron storage and the characteristics of long-range electron transport.

1. Quantum-dot solids

An insulating nanocrystal in the neutral ground state has completely filled valence energy levels and empty conduction levels. Insulating nanocrystals provided with one or more *extra* electrons, holes or excitons are often referred to as *artificial atoms*. An electron added to an otherwise neutral insulating crystal will occupy the conduction orbital of lowest energy (LUMO). This orbital is delocalized and must fit in the limited space of the nanocrystal; it has the same symmetry as an s-orbital in an conventional atom. The s-orbital can host a second electron with opposite spin. The third electron will occupy an orbital with p-type symmetry. Due to this quantum confinement, insulating nanocrystals possess a set of atom-like valence and conduction energy levels with energy separations which increase with decreasing dimensions. The energy separation between the discrete energy levels can be considerably larger than kT. The gap between the lowest conduction level (LUMO) and highest valence level (HOMO) also increases with decreasing dimensions. The fundamental optical transition can, therefore, vary in energy between the near IR and near UV. The tunability of the energy levels make nanocrystalline quantum-dots very promising building blocks for opto-electronic devices.

Colloidal nanocrystals can be assembled to form a solid. The van der Waals interactions between the surface and/or capping molecules are the driving force for self-assembly. If the nanocrystals have a spherical shape, and the size dispersion is below 5%, superlattices can be formed which show long-range order to a certain extent. Disordered assemblies and superlattices form the analogues of amorphous and crystalline conventional solids. The electronic properties of quantum-dot solids

will be determined by the energy levels of the individual nanocrystal building blocks and the degree of electronic coupling between the orbitals of adjacent quantum dots. The degree of electronic coupling depends on the effective mass of the charge carriers, and the distance between the nanocrystals in the assembly. The natural variation in the size of the nanocrystals and the distance between them in the assembly cause electronic disorder. Furthermore, the electrostatic energy needed to put a charge carrier in a nanocrystal, *i.e. the charging or electron–electron repulsion energy*, is another determinant of the electronic properties of a quantum-dot solid. The electrical properties of a quantum-dot solid thus depend on many degrees of freedom. Theoretical considerations have shown that this can lead to a rich palette of electrical regimes, including Anderson- and Mott-insulator/conductor transitions.[1] Electron conduction in a quantum-dot assembly implies that the electrons occupy the delocalized atom-like orbitals of the nanocrystal building blocks. The presence of one type of charge carriers, *i.e.* electrons, in a considerable density, requires compensation of the electronic charge by positively charged particles. Three-dimensional charge compensation in a quantum-dot solid is the main topic of this work.

2. Electron injection in a quantum-dot solid

We first consider the energetics of the addition of electrons, one by one, to an individual quantum dot.[2] The first extra electron will occupy the atom-like s-type conduction orbital of energy ε_s. The chemical potential of the electron source, needed to donate this electron to the quantum dot is:

$$\tilde{\mu}(0/1) = \varepsilon_s + E^{pol}, \tag{1}$$

here E^{pol} is the electrostatic polarization energy due to the dielectric mismatch between the quantum dot and the surroundings. In order to add a second electron to the nanocrystal, the chemical potential of the electron source must be increased with an amount E^{e-e} to overcome the Coulomb-repulsion energy with the electron already present in the quantum dot:

$$\tilde{\mu}(1/2) = \varepsilon_s + E^{pol} + E^{e-e}; \tag{2}$$

The third electron will occupy a p-type orbital. The chemical potential to add a third electron to the quantum dot is then:

$$\tilde{\mu}(2/3) = \varepsilon_p + E^{pol} + 2\ E^{e-e}. \tag{3}$$

The chemical potential for adding the fourth, fifth, and subsequent electrons is obtained in an analogous manner. It is instructive to compare this model for electron addition to a quantum dot with the conventional model for electron addition to a *metallic* nanocrystal. In a metallic crystal the level spacing is very small and is, usually, disregarded. From the above equations, it follows then that the chemical potentials for subsequent electron addition to a metal particle differ all by an amount E^{e-e} which is called the charging energy:

$$\tilde{\mu}(N/N+1) - \tilde{\mu}(N-1/N) = E^{e-e}. \tag{4}$$

In the constant-capacitance model, the electron–electron repulsion energy (electric charging energy) is given by:

$$E^{e-e} = \frac{e^2}{C}, \tag{5}$$

where C is the capacitance of the nanocrystal in a given configuration. The charging energy can vary over a wide range between 1 and 1000 meV, depending on the size of the nanocrystal, and the electrostatic coupling of the nanocrystal with the surroundings. In an electrical device with a single nanocrystal, embedded between two electrodes, the charging energy E^{e-e} leads to discrete single-electron transport through the device. This is often called the Coulomb blockade of electron transport.

We consider now electron addition to an assembly of insulating quantum dots. If the electronic coupling between the quantum dots is weak, electron addition occurs to a sample of "individual" quantum dots, thus, with energy levels which are not much changed by the electronic coupling.

Thus, we assume here that extended molecular orbitals do not occur. There is, however, a natural dispersion in the size of the quantum dots. As a consequence, not all quantum dots have the same electron occupation. Macroscopically, the occupation can be described by *the average number of electrons per quantum dot* $\langle n \rangle$. If the electrons in the assembly are in chemical equilibrium, $\langle n \rangle$ is decided by the electrochemical potential $\tilde{\mu}$ of the assembly. The charging characteristics are described by $\partial \langle n \rangle / \partial \tilde{\mu}$ (proportional to the differential capacitance) and $\langle n \rangle$ as a function of $\tilde{\mu}$. These depend on the quantised energy levels ε_s, ε_p, . . ., the charging energy E^{e-e}, and the variation of these parameters due to the dispersion in size of the quantum dots. The charging energy of a nanocrystal, isolated in vacuum, can be high, in the order of 500 meV[2]. Obviously, this limits the number of electrons that can be accommodated into one quantum dot. In order to obtain electron-conducting quantum-dot solids with a reasonable number of electrons, the electron–electron repulsion energy must be reduced. Here, we propose quantum-dot solids with *three-dimensional* charge compensation: the charge of the quantum-dot electrons is screened by positive charges present in the assembly. This method has, in fact, similarities to the doping of polymeric solids used to generate electron and hole conductivity. Three-dimension charge compensation will be discussed in the next section.

3. Three-dimensional charge compensation in a quantum-dot solid

There is a large scientific interest in electron-conducting solids. In the past, a field-effect set-up has often been used to generate a two-dimensional conducting layer in an insulating solid.[3] In this geometry, the active material is electrostatically coupled to a gate electrode. If a potential is applied between the active material and the gate, a two-dimensional layer of charge in the active material is formed which is compensated by the surface charge on the gate electrode. The charge density in the active material can reach 10^{12}–10^{13} charge units cm^{-2}. For a typical quantum dot assembly, consisting of nanocrystalline building blocks occupying sites 5 by 5 nm, the maximum number of electrons per quantum dot is then about one. A drawback in the use of the field-effect geometry, for the study of electron transport for instance, is that lattice defects and surface effects in the two-dimensional conductive layer can have a strong influence on the results and the reproducibility.

In a quantum-dot solid, excitons can be formed by optical excitation. The charge of each conduction electron is compensated by the positive charge of the hole. It has been reported that optical excitation of a solid of CdSe quantum dots leads to an increase of the electrical conductance.[4] However, the life-time of excitons in a quantum-dot solid is relatively short (maximum a few ns at room temperature) which leads to a small density of electrons and holes. In addition, it would be of interest to study quantum-dot solids with *only one type of charge carrier*. This is possible, in principle, by architectures in which electron-hole separation can occur. Fig. 1 (top) pictures an assembly of quantum dot-donor building blocks (Q–D): charge separation involves transfer of the hole from the photoexcited quantum dot to the donor-type unit resulting in a Q^-–D^+ state. Excitation of a donor-unit and subsequent electron transfer to the LUMO of the quantum dot gives the same charge-separated state. The life-time of the Q^-–D^+ charge-separated state can exceed the exciton-lifetime by orders of magnitude. It is thus expected that this method can lead to truly electron-hole conducting quantum-dot solids.

A second way to screen the charge of the electrons that occupy the quantum dots is by introducing *inert positive ions* in the pores of the assembly (Fig. 1 below-left). This is possible for a quantum-dot solid that can be permeated with a liquid electrolyte. This method of charge compensation can be employed in an electrochemical cell with a counter and a reference electrode, and the quantum-dot solid as work electrode. Electrochemically controlled electron storage in an assembly of CdSe quantum dots has been reported recently.[5] We employed this method to study electron storage and transport in assemblies of ZnO nanocrystals.[6] These nanocrystals are uncapped, and form assemblies which can be permeated with an electrolyte solution. It was possible to control the electron occupation of the ZnO quantum dots by the electrochemical potential and to study the characteristics of electron storage and electron transport (see experimental methods at the end). In the next sections we will focus on the intriguing and partly unexplained differences that were found between ZnO QD assemblies permeated with an *aqueous* or with an *aprotic* electrolyte solution.

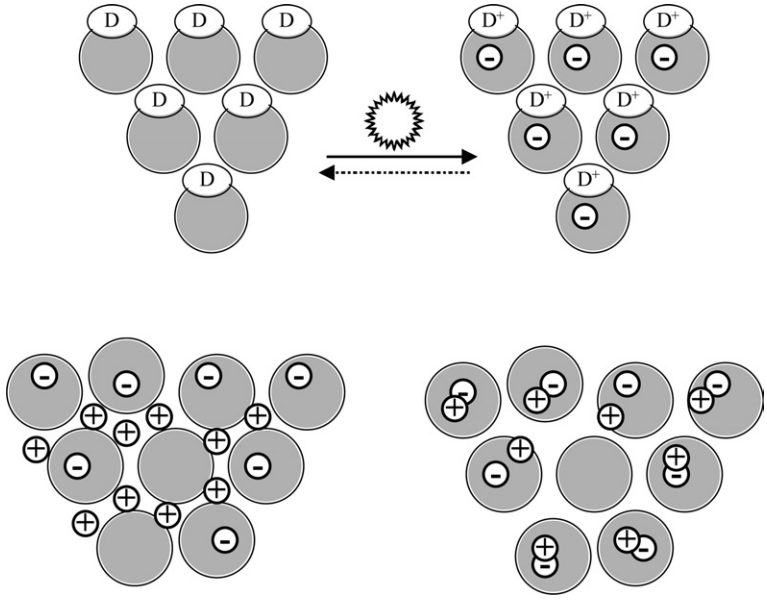

Fig. 1 Principles of three-dimensional charge compensation in a quantum-dot solid. *Above*: An ordered array consisting of quantum dot-donor building blocks. The system is insulating in the ground state. Upon photo-excitation of the quantum dot or the donor electron-hole separation occurs, leading to conduction electrons in the quantum dots; the charge is compensated by the photo-ionized donors. *Below-left*: An electron-conducting quantum-dot solid in which the charge of the electrons is compensated by positive ions (from an electrolyte solution) present in the pores of the assembly. *Below-right:* Protons can be strongly adsorbed on the quantum dots or, even, inserted into the nanocrystal lattice. This leads to a more efficient screening of electron–electron repulsion in the solid.

4. Electron-storage in a porous assembly of ZnO quantum dots

Fig. 2 presents the increase in the number of electrons per ZnO quantum dot, Δn, injected per 50 mV increase of the electrochemical potential of the assembly as a function of the accumulation

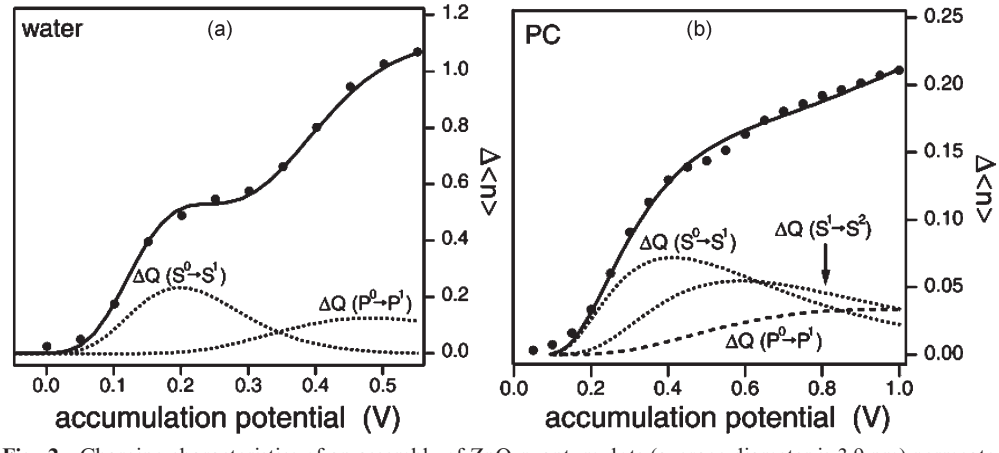

Fig. 2 Charging characteristics of an assembly of ZnO quantum dots (average diameter is 3.9 nm) permeated with an aqueous (a) and with propylene carbonate electrolyte solution (b). We present the increase of the electron number $\Delta\langle n\rangle$ for a 50 mV increase of the electrochemical potential as a function of the accumulation potential. The black dots are the measured values, the black lines are a fit based on a sum of single-electron addition functions, two of which shown as dotted and dashed lines.

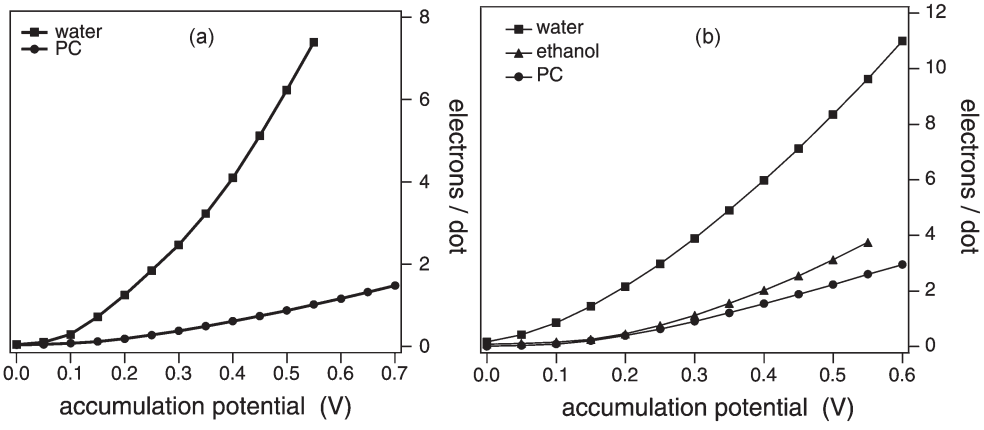

Fig. 3 Average number of electrons per quantum dot present in an assembly permeated with an aqueous, a propylene carbonate, and ethanol electrolyte solution as a function of the accumulation potential. (a) An assembly with ZnO nanocrystals of 3.9 nm in diameter. (b): An assembly with ZnO nanocrystals of 4.3 nm in diameter.

potential. The accumulation potential is the electrochemical potential referred to the potential of onset of electron injection given by eqn. (1); Δn is proportional to $\partial\langle n\rangle/\partial\tilde{\mu}$ and, thus, to the differential capacitance. Fig. 2a and b presents the charging characteristics of the same assembly permeated with an aqueous and a propylene carbonate electrolyte solution, respectively. Optical measurements show that all injected electrons occupy delocalized conduction orbitals, thus electron storage in surface states is not important.[6,7] With an aqueous electrolyte solution, the capacitance function $\partial\langle n\rangle/\partial\tilde{\mu}$ shows two steps. This corresponds to the injection of two electrons per quantum dot in the s conduction orbital (see eqn. (1)) followed by the injection of six electrons per quantum dot in the p-orbitals (see eqn. (2)). The capacitance function can be fitted using the energy levels ε_s and ε_p calculated by tight-binding theory and assuming that *the charging energy* E^{e-e} *is smaller than* kT. The two dotted curves in Fig. 2a give the single-electron capacitance functions for addition of the first electron to the s-orbitals and the third electron to the P-orbitals, respectively. The experimental data correspond to the sum of such single-electron functions (black full line). The broadening reflects the size-dispersion of the ZnO nanocrystals in the assembly. In contrast, the capacitance function obtained in propylene carbonate (Fig. 2b) can only be fitted by assuming that *the charging energy* E^{e-e} is 100 meV, *on average*. The single-electron functions for addition of the first and second electron are thus separated. They are also additionally broadened, resulting in a strong overlap with the single-electron function for addition of the third electron to a p-orbital. The charging energy of 100 meV found with propylene carbonate as a permeating solvent results in a considerably lower electron occupancy in the assembly of ZnO quantum dots. This is demonstrated in Fig. 3 which shows the average electron number as a function of the accumulation potential for an assembly permeated with an aqueous and with ethanol and propylene carbonate electrolyte solutions. The striking difference in the electron–electron repulsion energy observed in *water* ($E^{e-e} < kT$) and *aprotic solvents* (propylene carbonate, ethanol, acetonitrile) ($E^{e-e} \cong 3$–$5kT$) will be discussed below.

5. The characteristics of electron transport

As soon as electrons are injected into the assembly, the conductance measured between a source and drain electrode biased with a very small potential difference (1–10 mV) sets on promptly and increases by over four orders of magnitude with increasing electrochemical potential (Figs. 4a and b). The electron mobility can be derived from the geometry and the known electron density. The electron mobility is presented as a function of the accumulation potential in the insets. The two-wave function found in films permeated with an aqueous electrolyte has been discussed in a

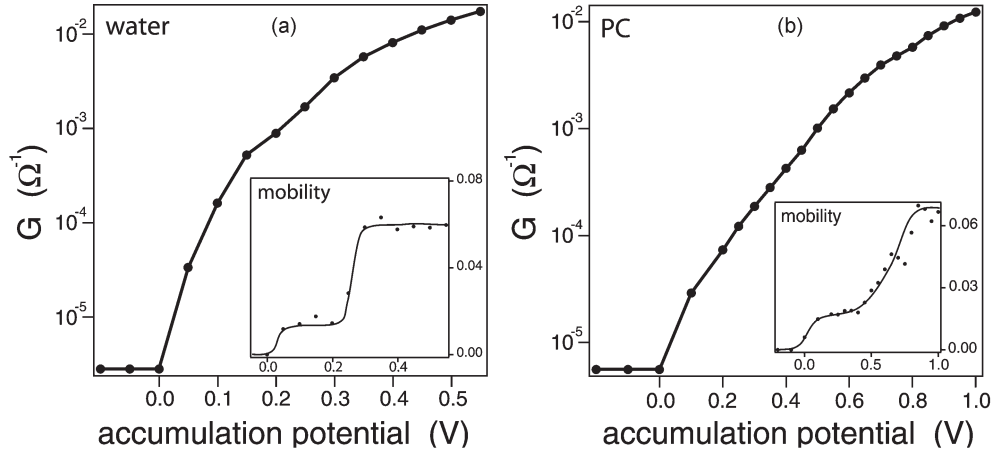

Fig. 4 Transport characteristics of an assembly of ZnO quantum dots (average diameter is 3.9 nm) permeated with an aqueous electrolyte solution (a) and with propylene carbonate (b). The conductance G is shown, measured between a source and drain electrode at room temperature, as a function of the accumulation potential. The insets show the electron mobility, derived from the conductance, electron density and geometrical parameters, as a function of the accumulation potential.

previous work. The first plateau in the mobility corresponds to $0 < \langle n \rangle < 2$ and is due to electron motion by subsequent tunneling between the s-type delocalized orbitals. Tunneling between p-type conduction orbitals prevails in the second plateau. There is a transition region between the two regimes due to the size distribution in the assembly. We found that the conductance was independent of the temperature in the range 280–310 K. Transport through a ZnO nanocrystal assembly permeated with water is thus decided by the quantum confined energy levels of the building blocks and the electronic coupling between them. Although the value of the mobility shows clearly that electron transport is not coherent, there is no Coulomb blockade of transport. This agrees with the low value of the electron–electron repulsion energy observed in the electron storage characteristics.

Again, assemblies permeated with an aprotic solvent behave differently. There is a plateau in the mobility *vs.* accumulation potential (inset of Fig. 4b) but the mobility rises further as soon as $\langle n \rangle$ exceeds $1/2$. We conjecture that in this case both s- and p-orbitals are involved in electron transport. This is based on the strong overlap of the single-electron addition functions to the s- and p-orbitals demonstrated in the capacitance function (Fig. 2b). We have studied the temperature-dependence of electron transport by measuring the source-drain conductance in a range between room temperature and the melting point of the aprotic electrolyte solutions (propylene carbonate and ethanol) that permeate the assembly. The conductance increases exponentially with the temperature, the thermal activation energy was between 80 and 120 meV. These activation energies are close to the electron–electron repulsion energy observed from the capacitance function (Fig. 2b). Thus, the temperature dependence points to Coulomb blockade of electron transport originating from the Coulomb repulsion energy between the electrons, E^{e-e}, having a value around 100 meV.

6. Why is screening of the electron charge so efficient when the assembly is permeated with water?

Coulomb blockade of electron transport through a nanodevice consisting of a single active molecule, or a metallic or insulating nanocrystal has been observed at temperatures at which the electric charging energy E^{e-e} exceeds kT. Temperature-activated long-range transport through molecular crystals and superlattices of metallic and insulating quantum dots has also been attributed to Coulomb blockade. The rationalization is that, each time the electron hops from a given unit to the adjacent unit in the assembly, the Coulomb repulsion energy E^{e-e} has to be overcome by thermal energy. With increasing temperature, the effects of Coulomb blockade fade as

soon as $2kT \geq E^{e-e}$. In the assemblies of ZnO quantum dots permeated with an aprotic electrolyte solution considered in this work, electric charging of the ZnO quantum dots plays an important role in electron storage and long-range transport. In contrast, if the assembly is permeated with an aqueous electrolyte solution, the charging energy is not visible in the characteristics of electron storage and transport, which means that $E^{e-e} \leq 2kT$. *Why is screening of the electron charge in the ZnO quantum dots so efficient in the case of the aqueous electrolyte?* We have observed that the charging energy is independent of the nature and the size of the cation used in the electrolyte. This means that mechanical aspects of ion permeation in the pores of the assembly play no role. In addition, the small differences in the dielectric constant of the solvents that we have used cannot explain the difference between water and the other solvents. We speculate that the presence of protons in water is important here. Protons, with their small size, can be strongly adsorbed on the ZnO surface and might even be inserted into the ZnO lattice (Fig. 1-below-right). Hence, the delocalised electron orbitals can overlap strongly with the proton. As a result, there is screening of the electron charge *inside the quantum dot* and, thus, a strong reduction of the electron–electron repulsion energy E^{e-e}. This situation is somewhat similar to that of an exciton in a quantum dot: in this case, the polarization energies of electron and hole are nearly compensated by the electron-hole attraction energy. Ions present in the pores, between the quantum dots, are less efficient in the screening of the electron–electron repulsion (Fig. 1, below-left).

7. Outlook

Artificial solids show similarities to conventional solids but, electronically, they are more complex and, in addition, inherently disordered. Electron (hole) conducting quantum-dot solids can be considered as a collection of artificial atoms in which the atomic number, the confinement energies, and inter-atomic coupling are important degrees of freedom. Research on the electronic properties of these systems has just been started. Quantum-dot solids (CdSe and ZnO) with electrochemical electron injection and ionic charge compensation have proven to be very valuable for basic research. Quantum-dot solids which possess long-range order in the nanocrystal configuration may form a true equivalent of conventional crystals. We hope that more research groups will enter this challenging field in the near future.

Experimental

The synthesis of the colloidal ZnO nanocrystals has been described elsewhere.[6] The particle size of the washed ZnO quantum dots was determined with X-ray diffraction (XRD) and transmission electron microscopy (TEM). The maximum error which is made in the determination of the diameter of the quantum dots with TEM and XRD is estimated to be 15%.

Transparent films of pure wurtzite ZnO quantum dots were made by spin-coating the solution of ZnO particles on a conducting substrate. The film was heated after each spin-coating step for 15 min to remove the solvent. Low temperatures (90–110 °C) were used to prevent neck formation between the dots. The low temperature and the thorough washing procedure of the sol are necessary to observe the phenomena which are described in the present work. Very flat and optically transparent films are formed with this technique. The thickness of the quantum dot films, about 200 nm, was obtained by profilometry (Tencor Instruments alpha-step 500). The absorption spectrum of the ZnO layer shows a slight red-shift with respect to the absorption spectrum of the original washed ZnO sol. This confirms that the quantum properties of the individual ZnO nanocrystals are preserved in the film.

The zinc and lithium content of the films were determined by inductively coupled plasma optical emission spectrometry (ICP-OES) after dissolution of the films in diluted HCl. This chemical analysis showed that lithium was not present above its detection limit (0.5 atom% relative to zinc) after the washing procedure. From the amount of ZnO and the average volume per quantum dot the number of quantum dots in the film is estimated. From this number and the injected charge, the average number of electrons per dot $\langle n \rangle$ is obtained. The maximum uncertainty in $\langle n \rangle$ is 50%.

For the measurements of the long-range transport, gold source- and drain-electrodes were used (30 nm thick gold deposited on a 5 nm thick adhesion layer of chromium on a flat glass substrate) with a non-conducting gap of 10 μm wide and 1 cm long.

The aqueous electrolyte was an argon-purged 0.2 M phosphate buffer (pH = 8) and was made by adding pure NaOH to phosphoric acid. Here the reference electrode was a Ag/AgCl electrode, and the counter electrode a platinum sheet. Otherwise, anhydrous propylene carbonate (PC) with 0.1 M tetrabutylammonium perchlorate ($TBAClO_4$) was used. In this electrolyte a silver rod served as a quasi-reference electrode calibrated with the ferrocene/ferrocinium couple: the potential was found to be ~200 mV *vs.* Ag/AgCl. The experiments in ethanol or propylene carbonate solvents were carried out in a nitrogen-filled glovebox in order to keep the solutions free of oxygen and water. The ethanol and propylene carbonate were used without further purification. The water content of the pure solvents was 0.2% and 0.3%, respectively.

Acknowledgements

We wish to thank Dr J.-N. Chazalviel (Ecole Polytechnique, Palaiseau) for useful discussions.

References

1 F. Remacle and R. D. Levine, *ChemPhysChem*, 2001, **2**, 20.
2 A. Franceschetti, A. Williamson and A. Zunger, *J. Phys. Chem. B*, 2000, **104**, 3398.
3 W. A. Schoonveld, J. Wildeman, D. Fichou, P. A. Bobbert, B. J. Van Wees and T. M. Klapwijk, *Nature*, 2000, **404**, 977.
4 D. S. Ginger and N. C. Greenham, *J. Appl. Phys.*, 2000, **87**, 1361.
5 C. J. Wang, M. Shim and P. Guyot-Sionnest, *Appl. Phys. Lett.*, 2002, **80**, 4.
6 A. L. Roest, J. J. Kelly, D. Vanmaekelbergh and E. A. Meulenkamp, *Phys. Rev. Lett.*, 2002, **89**, 36 801.
7 A. Germeau, A. L. Roest, D. Vanmaekelbergh, G. Allan, C. Delerue and E. A. Meulenkamp, *Phys. Rev. Lett.*, 2003, **90**, 97 401.